

# PCCP

Accepted Manuscript



This is an *Accepted Manuscript*, which has been through the Royal Society of Chemistry peer review process and has been accepted for publication.

*Accepted Manuscripts* are published online shortly after acceptance, before technical editing, formatting and proof reading. Using this free service, authors can make their results available to the community, in citable form, before we publish the edited article. We will replace this *Accepted Manuscript* with the edited and formatted *Advance Article* as soon as it is available.

You can find more information about *Accepted Manuscripts* in the [Information for Authors](#).

Please note that technical editing may introduce minor changes to the text and/or graphics, which may alter content. The journal's standard [Terms & Conditions](#) and the [Ethical guidelines](#) still apply. In no event shall the Royal Society of Chemistry be held responsible for any errors or omissions in this *Accepted Manuscript* or any consequences arising from the use of any information it contains.

## Theoretical study on the molecular determinants of the affibody protein $Z_{A\beta 3}$ bound to an amyloid $\beta$ peptide

Cite this: DOI: 10.1039/x0xx00000x

Xu Wang, Xianqiang Sun, Guanglin Kuang, Hans Ågren, and Yaoquan Tu\*

Received 00th January 2012,  
Accepted 00th January 2012

DOI: 10.1039/x0xx00000x

[www.rsc.org/](http://www.rsc.org/)

Amyloid beta ( $A\beta$ ) peptides are small cleavage products of the amyloid precursor protein. Aggregates of  $A\beta$  peptides are thought to be linked with Alzheimer's and other neurodegenerative diseases. Strategies aimed at inhibiting amyloid formation and promoting  $A\beta$  clearance have been proposed and investigated in *in vitro* experiments and *in vivo* therapies. A recent study indicated that a novel affibody protein  $Z_{A\beta 3}$ , which binds to an  $A\beta 40$  monomer with a binding affinity of 17 nM, is able to prevent the aggregation of  $A\beta 40$ . However, little is known about the energetic contribution of each residue in  $Z_{A\beta 3}$  to the formation of the  $(Z_{A\beta 3})_2:A\beta$  complex. To address this issue, we carried out unbiased molecular dynamics simulations and molecular mechanics Poisson-Boltzmann surface area calculations. Through the per-residue decomposition scheme, we identified that the van der Waals interactions between the hydrophobic residues of  $(Z_{A\beta 3})_2$  and those at the exterior and interior faces of  $A\beta$  are the main contributors to the binding of  $(Z_{A\beta 3})_2$  to  $A\beta$ . Computational alanine scanning identified 5 hot spots, all residing in the binding interface and contributing to the binding of  $(Z_{A\beta 3})_2$  to  $A\beta$  through the hydrophobic effect. In addition, the amide hydrogen bonds in the 4-strand  $\beta$ -sheet and the  $\pi$ - $\pi$  stacking were also analyzed. Overall, our study provides a theoretical basis for future experimental improvement of the  $Z_{A\beta 3}$  peptide binding to  $A\beta$ .

### Introduction

Alzheimer's disease (AD) is a neurodegenerative disorder and the most common cause of late-life dementia<sup>1</sup>. The pathological hallmark of AD is the senile plaques comprising primarily fibrils of amyloid beta ( $A\beta$ ) peptides in the brains of AD patients<sup>2, 3</sup>.  $A\beta$  peptides are small cleavage products of the amyloid precursor protein (APP). They vary in lengths ranging from 39 to 43 amino acid residues, of which  $A\beta 40$  is the most abundant peptide while  $A\beta 42$  is supposed to be most neurotoxic<sup>4, 5</sup>. Although deposition of amyloid fibrils in plaques has been observed, multiple lines of evidence indicate that small, soluble, and more toxic oligomers of  $A\beta$  peptides are responsible for the synaptic and cognitive dysfunction<sup>6-8</sup>. Intermediate oligomers are also believed to serve as seeding nuclei for the growth of amyloid fibrils<sup>9</sup>.

Different strategies aimed at decreasing the amount of  $A\beta$  peptides in the brain, such as reducing their production, inhibiting their

accumulation and oligomerization, or promoting their clearance, have been investigated<sup>10</sup>. One important strategy is to use immunotherapy to treat AD by stimulating the clearance of  $A\beta$  from the brain of AD patients via anti- $A\beta$  antibodies. AN1792, the first active immunotherapy vaccine for AD, has shown to be promising in preclinical animal studies<sup>11</sup>. However, this vaccine was abandoned due to the occurrence of meningoencephalitis in approximately 6% of the treated patients<sup>12, 13</sup>. Another immunological approach is passive immunization using anti- $A\beta$  monoclonal antibodies. Bapineuzumab, for example, is such an anti- $A\beta$  monoclonal antibody that targets the N-terminus of  $A\beta$ . It has been tested in the early clinic trials and proven to reduce the  $A\beta$  burden in the brain of AD patients<sup>14, 15</sup>. However, two very recent Phase III trials demonstrated that it fails to improve clinical outcomes in patients with mild to moderate AD<sup>16</sup>. Although the progress of these studies is not satisfactory, particularly in view of the urgent need for ways to treat AD, targeting and clearing  $A\beta$  remains a promising method to treat people suffering from this disease.

Recently, a novel affibody peptide,  $Z_{A\beta 3}$ , prepared based on the engineered Z domain originating from the B domain of staphylococcal protein A has attracted much attention<sup>17</sup>. This peptide is designed to target monomeric A $\beta$ 40 with a binding affinity of 17 nM<sup>18</sup>. Co-expressions of  $Z_{A\beta 3}$  and A $\beta$  peptides in the brain of *Drosophila melanogaster* prevent the neuronal damage and premature death caused by the expression of A $\beta$  peptides alone<sup>19</sup>. *in vitro* experiments have shown that  $Z_{A\beta 3}$  not only occludes the initial aggregation of A $\beta$  monomers into toxic forms, but also functions to dissociate the pre-formed oligomeric aggregates<sup>19, 20</sup>. Structural analysis of  $Z_{A\beta 3}$  in complex with A $\beta$ 40 reveals that  $Z_{A\beta 3}$  is a head-to-tail homodimer. The complex has the feature that the  $\beta$ -hairpin structure composed of residues 17-36 of A $\beta$ 40 is in a large hydrophobic tunnel-like cavity formed by  $Z_{A\beta 3}$ . Residues 1-13 of each  $Z_{A\beta 3}$  subunit are disordered and are not involved in binding to the A $\beta$  monomer, while residues 15-18 form a  $\beta$ -strand that flanks on a side of the A $\beta$  hairpin, allowing the complex to form a four-stranded antiparallel  $\beta$ -sheet through intra-molecular and intermolecular hydrogen bonds. The  $\beta$ -sheet is further anchored against helix 3 of the affibody by forming a salt bridge between Glu15 and Lys49 in each of the affibody subunits<sup>20</sup>.

In view of the potential application of  $Z_{A\beta 3}$  in *in vivo* therapy, it is worthwhile to carry out studies on enhancing the affinity of  $Z_{A\beta 3}$  binding to A $\beta$  through mutating or truncating undesired residues. Studies have been carried out on improving the binding of  $Z_{A\beta 3}$  to A $\beta$  through rational truncations of the N-termini on each subunit<sup>21, 22</sup>. However, little is known about the energetic contribution of each residue in  $Z_{A\beta 3}$  to its binding to A $\beta$ . Understanding this issue would help us to guide future experimental investigations aimed at improving the affinity of  $Z_{A\beta 3}$  to A $\beta$  peptides.

In this work, we carried out molecular dynamics (MD) simulations together with employing the Molecular Mechanics Poisson-Boltzmann Surface Area (MM-PBSA) approach<sup>23</sup> to explore the molecular basis of the  $(Z_{A\beta 3})_2$  protein binding to the A $\beta$  peptide. MM-PBSA is an implicit solvent free energy estimation method that has been widely used in a number of studies due to its relatively low computational cost and reasonable accuracy in evaluating binding free energies for various molecular systems<sup>24-26</sup>. The per-residue decomposition method in MM-PBSA allows us to distribute the effective binding free energy for the  $(Z_{A\beta 3})_2$ :A $\beta$  complex at the residue level. With this method, we can determine the contribution of each  $Z_{A\beta 3}$  residue to its binding to A $\beta$  and understand the origin of the interactions between  $(Z_{A\beta 3})_2$  and A $\beta$ . We also carried out computational alanine scanning to identify the hot spots of  $Z_{A\beta 3}$ . Finally, some important non-covalent interactions, for example amide H-bonds and  $\pi$ -stacking, involved in stabilizing  $(Z_{A\beta 3})_2$  in complex with A $\beta$  were analyzed. This work thus provides a detailed study of the  $(Z_{A\beta 3})_2$ :A $\beta$  complex and explores the role of the  $Z_{A\beta 3}$  residues in the complex. We believe that this study can serve as a basis for future experimental improvements of the  $(Z_{A\beta 3})_2$  protein binding to A $\beta$ .

## Computational Methods

### System setup and the MD simulations

The NMR structure of the protein complex formed by the dimeric  $Z_{A\beta 3}$  and A $\beta$ 40 (PDB code: 2OTK)<sup>20</sup> was used as the initial structure for the MD simulations. The N-terminal fragments containing residues 1-15 of A $\beta$ 40 and 1-13 of each affibody subunit were not included in the simulations, as these residues have been proved to be disordered and contribute little

to the complex formation. Based on visual inspection and PROPKA<sup>27</sup>, His32 in each  $Z_{A\beta 3}$  subunit was protonated at the N $_{\delta}$  and N $_{\epsilon}$  positions of the imidazole ring. The protonation states of other histidine residues were set according to their local environment. The protonation states for the charged residues, such as Asp, Glu, Arg and Lys, were kept as default. The total charge for the protein complex is thus -7|e|.

The MD simulations were carried out using the Gromacs/4.6.3 simulation program<sup>28</sup>, with the Amber ff99SB force field<sup>29</sup> to model the interactions between the peptide atoms. The protein complex was placed in a cubic box of 65×65×65 Å<sup>3</sup> and solvated with 8714 TIP3P<sup>30</sup> water molecules. Seven Na<sup>+</sup> ions were added into the box to neutralize the system. The resulting system was then subject to 5000 steps of steepest descent minimization. The periodic boundary condition was applied in the simulation. The cut-off distances for the Lennard-Jones and electrostatic interactions were set to 10 Å. The electrostatic interactions beyond the cut-off were recovered by the Particle Mesh Ewald (PME) summation method. The system was heated to 300 K in 100 ps by using the v-rescale thermostat<sup>31</sup>. During this process, the Linear Constraint Solver (LINCS) algorithm<sup>32</sup> was used to constrain all the bond lengths. The isothermal isobaric ensemble (NPT) was used in the subsequent simulations, with the pressure set to 1 bar, controlled by the Parrinello-Rahman barostat<sup>33</sup>. The system was first simulated for 1 ns. In the above equilibration stages, a harmonic restraint with the force constant of 1000 kJ/(mol·nm<sup>2</sup>) was applied to all the heavy atoms of the complex to constrain the protein complex. Thereafter, the restraining forces on the heavy atoms were removed and the system was simulated for 200 ns. Three repeated MD simulations with different initial velocities were also performed. Throughout the simulations a time step of 2.0 fs was used. The trajectory of each simulation was recorded every 5000 time steps (10.0 ps), with the last 10 ns of the trajectory chosen for the MM-PBSA calculation.

### Effective binding free energy and per-residue contributions

The calculation of the effective binding free energy between  $(Z_{A\beta 3})_2$  and A $\beta$ 16-40 was performed using the post-processing module MM-PBSA in the Amber 12 package<sup>34</sup>, based on the snapshots taken from the MD simulations. Water molecules and counter ions were stripped from the snapshots.

For a protein complex consisting of protein A and protein B, the binding free energy can be calculated based on the following equation,

$$\Delta G_{bind} = G_{complex} - G_A - G_B \\ = \Delta E_{MM} + \Delta G_{solv} - T\Delta S,$$

where  $G_{complex}$ ,  $G_A$ , and  $G_B$  are the free energies of the complex, protein A and protein B, respectively.  $\Delta E_{MM}$  is the gas-phase interaction energy between protein A and protein B,  $\Delta G_{solv}$  is the change of the solvation free energy of the system due to the complex formation, and the  $-T\Delta S$  term is the solute entropy contribution originating from the change of the degrees of freedom. The  $-T\Delta S$  term is mainly related to the change of the vibrational entropies upon protein A binding to protein B, which was not considered in our work because of the large uncertainty in estimating the vibrational entropy contributions<sup>35, 36</sup> (we will discuss this term in detail later). Therefore, in our MM-PBSA calculations, we only considered the “effective binding energies” ( $\Delta G_{eff}$ ),

$$\Delta G_{eff} = \Delta E_{MM} + \Delta G_{solv},$$

where  $\Delta E_{MM}$  includes the molecular mechanics energy contributed by the bonded ( $\Delta E_{bond}$ ,  $\Delta E_{angle}$ ,  $\Delta E_{torsion}$ ) and nonbonded ( $\Delta E_{vdw}$  and  $\Delta E_{elec}$ ) terms, with

$$\Delta E_{MM} = \Delta E_{bond} + \Delta E_{angle} + \Delta E_{torsion} + \Delta E_{vdw} + \Delta E_{elec}$$

In the single trajectory approximation, the bonded contribution to  $\Delta E_{MM}$  is zero because of the cancellation of the intramolecular interactions.  $\Delta G_{solv}$  was modeled as the sum of the electrostatic contribution ( $\Delta G_{elec,solv}$ ) and a nonpolar one ( $\Delta G_{np,solv}$ ),

$$\Delta G_{solv} = \Delta G_{elec,solv} + \Delta G_{np,solv}.$$

where  $\Delta G_{elec,solv}$  was calculated by solving the Poisson-Boltzmann (PB) equation with a finite-difference method. The nonpolar solvation free energy was computed as the sum of a favorable energy ( $\Delta G_{dis}$ , approximated as the van der Waals attractive interaction energy between the solute and solvent) and an unfavorable energy due to the cavity formation ( $\Delta G_{cav}$ )<sup>24, 37</sup>,

$$\Delta G_{np,solv} = \Delta G_{dis} + \Delta G_{cav},$$

with  $\Delta G_{cav}$  approximated by the empirical relationship,

$$\Delta G_{cav} = \gamma \Delta S_A + b,$$

where  $\gamma$  is the surface tension,  $\Delta S_A$  is the difference in the solvent accessible surface areas between the complex and the individual peptides, and  $b$  is the regression offset for the linear relationship. In this work, all the terms in the above equations are approximated as the mean values over the snapshots from the MD simulations of the complex.

For each snapshot,  $\Delta E_{MM}$  was calculated based on the ff99SB force field without applying any cutoff,  $\Delta G_{elec,solv}$  was determined by solving the linearized PB equation using the optimized atomic radii<sup>38</sup> and a solvent probe radius of 1.4 Å, according to a cubic lattice of length equaling to 4 times of the longest linear dimension of the molecule, at a grid spacing of 0.5 Å. For the computation of the attractive term  $\Delta G_{dis}$ , the radius of the solvent probe was set to 0.557 Å. For the  $\Delta G_{cav}$  evaluation, the empirical constants,  $\gamma$  and  $b$ , were set to 0.0378 kcal/(mol·Å<sup>2</sup>) and -0.5692 kcal/mol, respectively. The dielectric constants for the interior and exterior of a solute were 1 and 80, respectively, and a total of 1000 iteration steps were requested for a convergence criterion of 0.001 kT/e.

To obtain the molecular determinants of  $(Z_{A\beta 3})_2$  binding to A $\beta$ 40, the effective binding energies were further decomposed into the contribution from individual residues by using the MM-PBSA decomposition scheme<sup>39</sup>.

### Computational alanine/glycine scanning

The computational alanine scanning method involves truncating the side chain of a given residue (except glycine or proline), replacing its C $_{\gamma}$  atom with a hydrogen atom at the corrected distance along the former C $_{\beta}$ -C $_{\gamma}$  bond, and recalculating the absolute binding free energy of the mutated system. In this work, the binding free energy of the alanine mutant was calculated with the MM-PBSA approach described above, using the snapshots for the wild type complex. The entropy term, which includes the contributions from the transitional, rotational, and vibrational motions, was not considered because it is believed that this term contributes little to the difference in the

binding free energies between the mutant and wild type complexes,  $\Delta \Delta G_{bind}$ , and can be neglected safely<sup>40</sup>.  $\Delta \Delta G_{bind}$  can thus be expressed as

$$\Delta \Delta G_{bind} = \Delta G_{eff}^{mutant} - \Delta G_{eff}^{wild\ type}$$

Glycine scanning on the alanine residues of  $(Z_{A\beta 3})_2$  was also performed by truncating at the C $_{\beta}$  atom, similar to what is done in the computational alanine scanning method. Although glycine scanning cannot be compared quantitatively with alanine scanning, it allows us to compare the contribution of each alanine residue to the binding of  $(Z_{A\beta 3})_2$  to A $\beta$ 40.

## Results and Discussion

### Convergence of the MD simulations and changes of the local structure of the $(Z_{A\beta 3})_2$ :A $\beta$ complex

The convergence of the MD simulations was monitored by the root mean square deviations (RMSDs) of the structures of the complex and its components with respect to their initial structures obtained at the end of the minimization, respectively. In the first MD simulation, the RMSD of the heavy atoms in  $(Z_{A\beta 3})_2$ :A $\beta$  went rapidly up to 1.5 Å and gradually rose to 3.5 Å in the next 40 ns. After that it reduced to 3 Å and remained almost unchanged in the remaining simulation (**Fig. 1a**).  $(Z_{A\beta 3})_2$  has a rather similar RMSD trend to that of  $(Z_{A\beta 3})_2$ :A $\beta$ , whereas the smaller RMSD values along the trajectory indicate that  $(Z_{A\beta 3})_2$  is more stable and rigid than the protein complex  $(Z_{A\beta 3})_2$ :A $\beta$ . A $\beta$ , on the contrary, has larger conformational changes, as it has a smaller number of residues which results in the RMSD values being sensitive to the changes of the terminal residues and loop regions. Three repeated MD simulations also demonstrated a similar converging behaviour (**Fig. S1**).

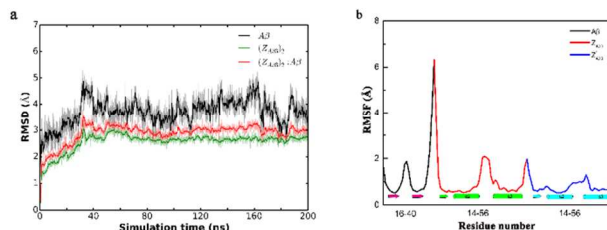


**Figure 1.** (a) The RMSD of the heavy atoms with respect to the structures obtained from the energy minimization. (b) The root mean square fluctuation (RMSF) of each residue in  $(Z_{A\beta 3})_2$ :A $\beta$ . The  $\beta$ -strands and  $\alpha$ -helices in  $(Z_{A\beta 3})_2$ :A $\beta$  are indicated by the arrows and cylinders, respectively.

To find out the structural flexibility of each component in the  $(Z_{A\beta 3})_2$ :A $\beta$  complex, the root mean square fluctuations (RMSFs) of the backbone atoms in each of the complex residues were calculated (**Fig. 1b**). The RMSFs for the four antiparallel  $\beta$ -strands and the  $\alpha$ -helices were as low as  $\sim$ 0.8 Å, indicating that these secondary structures are stable and rigid. The RMSF profile also indicates that the residues with higher fluctuation values are those located in the loop or turn regions, or at the N-/C- termini of each polypeptide in the complex. From the RMSF values, we can see that the structure fluctuation origins primarily from the loop or terminal residues in the complex, while the functionally relevant structures are quite conserved in the simulation.

**Table 1.** Effective binding free energy for  $(Z_{A\beta 3})_2$  binding to  $A\beta$ 

	$\langle \Delta E_{vdw} \rangle$	$\langle \Delta E_{elec} \rangle$	$\langle \Delta G_{elec,solv} \rangle$	$\langle \Delta G_{cav} \rangle$	$\langle \Delta G_{dis} \rangle$	$\langle \Delta G_{eff} \rangle$
MM-	-120.56	-223.84	248.87	-91.08	160.97	-25.64
PBSA	(2.47)	(41.84)	(42.15)	(1.47)	(2.98)	(1.20)

The energy unit is in kcal/mol. The brackets denote an average over the last 10 ns of the MD simulations. Values in the parentheses are the standard deviations for the corresponding mean values.

**Table 2.** Per-residue contributions to the effective binding energies calculated with the MM-PBSA method

Residue	$\langle \Delta \Delta E_{vdw} \rangle$	$\langle \Delta \Delta E_{elec} \rangle$	$\langle \Delta \Delta G_{elec,solv} \rangle$	$\langle \Delta \Delta G_{cav}^{bb} \rangle$	$\langle \Delta \Delta G_{dis}^{sc} \rangle$	$\langle \Delta \Delta G_{eff} \rangle$
$Z_{A\beta 3}$ Glu15	-2.18	-1.59	2.19	-1.51	-0.07	-1.58
$Z_{A\beta 3}$ Ile16	-3.03	-1.48	1.33	-1.50	-1.68	-3.18
$Z_{A\beta 3}$ Val17	-2.23	-4.22	3.82	-1.54	-1.09	-2.63
$Z_{A\beta 3}$ Tyr18	-3.20	-11.75	9.00	-0.99	-4.96	-5.95
$Z_{A\beta 3}$ Leu19	-2.07	-2.74	3.09	-0.58	-1.14	-1.72
$Z_{A\beta 3}$ Pro20	-1.50	-0.66	0.95	-0.69	-0.52	-1.21
$Z_{A\beta 3}$ Leu27	-1.21	-0.53	0.53	-0.33	-0.88	-1.21
$Z_{A\beta 3}$ Leu45	-1.66	0.29	-0.19	-0.26	-1.30	-1.56
$Z_{A\beta 3}$ Ile16	-3.29	-2.03	1.06	-1.82	-2.44	-4.26
$Z_{A\beta 3}$ Val17	-1.61	-3.73	2.71	-1.59	-1.04	-2.63
$Z_{A\beta 3}$ Tyr18	-3.93	-0.94	2.31	-0.86	-1.70	-2.56
$Z_{A\beta 3}$ Leu19	-2.43	-3.21	3.33	-0.84	-1.47	-2.31
$Z_{A\beta 3}$ Pro20	-1.75	-2.44	2.73	-0.91	-0.55	-1.46
$Z_{A\beta 3}$ Leu27	-1.23	0.88	-0.91	-0.24	-1.02	-1.26
$Z_{A\beta 3}$ Leu45	-2.40	-1.66	1.65	-0.16	-2.25	-2.41

Only residues in  $(Z_{A\beta 3})_2$  with favourable energy contributions are listed ( $\Delta \Delta G_{eff} < -1.20$  kcal/mol). The energies are in kcal/mol. The brackets denote an average over the last 10 ns of the MD simulation trajectories. <sup>a</sup>The effective binding energy  $\Delta \Delta G_{eff}$  contributed by each residue does not include the contribution from the nonpolar solvation free energy as it is currently not decomposable in the MM-PBSA method. Therefore,  $\Delta \Delta G_{eff}$  for each residue equals to the sum of the  $\Delta \Delta E_{vdw}$ ,  $\Delta \Delta E_{elec}$  and  $\Delta \Delta G_{elec,solv}$  terms as well as to the sum of the backbone ( $\Delta \Delta G_{cav}^{bb}$ ) and side chain ( $\Delta \Delta G_{dis}^{sc}$ ) contributions.

### Effective binding free energy calculations and per-residue contributions

The effective binding energy was calculated using the MM-PBSA method, based on the last 10 ns of the MD simulation trajectories. To evaluate the convergence of the averaged energy components, standard errors for these energy components were computed and were found to range from 0.12 to 0.91 kcal/mol, indicating that the last 10 ns of the trajectories were sufficient for the effective energy estimations. With the MM-PBSA method, we obtained an effective binding energy of -25.64 kcal/mol for  $(Z_{A\beta 3})_2$  binding to  $A\beta$ , suggesting that the formation of the  $(Z_{A\beta 3})_2:A\beta$  complex is energetically favourable (Table 1). For the binding of  $(Z_{A\beta 3})_2$  to  $A\beta$ ,  $\Delta G_{dis}$  is energetically unfavourable while  $\Delta G_{cav}$  is energetically favorable. The resulting  $\Delta G_{np,solv}$  is therefore energetically unfavourable due to the overwhelming contribution of the  $\Delta G_{dis}$  term. The effective binding energy can be further approximately decomposed at a per-residue basis so that we can find out which residue or even which part of a residue in  $(Z_{A\beta 3})_2$  plays important roles in the binding of  $(Z_{A\beta 3})_2$  to  $A\beta$ .

The binding entropy can be computed through either normal mode or quasiharmonic analyses. Nevertheless, the binding entropy was not considered here, because the aim of this work is to identify residues that play important roles in stabilizing the  $(Z_{A\beta 3})_2:A\beta$  protein complex. Moreover, the normal mode analysis method does not take into account the anharmonic contributions, which probably leads to systematic errors in calculating the vibrational entropy term, whereas the

quasiharmonic method suffers from the convergence of the entropy estimation<sup>41</sup>.

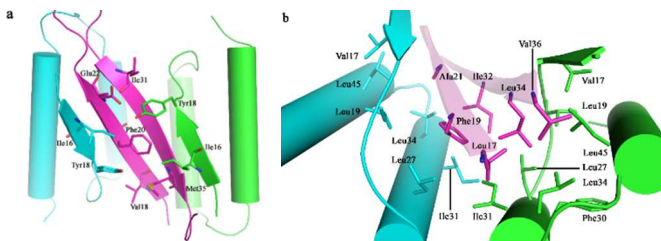


**Figure 2.**  $(Z_{A\beta 3})_2$  residues with favorable  $\Delta \Delta G_{eff}$  for the binding of  $(Z_{A\beta 3})_2$  to  $A\beta$ . The hydrophobic residues of each subunit interact with either the exterior face (a) or the interior face (b) of the  $A\beta$  residues. The cartoon representations of  $A\beta$ , the  $Z_{A\beta 3}$  and  $Z'_{A\beta 3}$  subunits are rendered in magenta, green and cyan, respectively.

Here, we further study the energetic contributions of the affinity residues to its binding to  $A\beta$ . Residues of  $(Z_{A\beta 3})_2$  with effective energy contributions ( $\Delta \Delta G_{eff}$ ) lower than -1.20 kcal/mol are listed in Table 2. It should be noted that since the  $\Delta G_{np,solv}$  term in the total effective binding energy is indecomposable, the  $\Delta \Delta G_{eff}$  value for each residue is in fact the sum of the  $\Delta \Delta E_{vdw}$ ,  $\Delta \Delta E_{elec}$  and  $\Delta \Delta G_{elec,solv}$  terms, and does not include the contribution from the energetically unfavourable  $\Delta \Delta G_{np,solv}$  term. Therefore,  $\Delta \Delta G_{eff}$  of a residue overestimates its real contribution to the total effective binding energy. However, we believe that this will not affect our evaluation of the relative importance of the residues in binding to the  $A\beta$  peptide. With the exception of Glu15 in  $Z'_{A\beta 3}$ , residues Glu15, Ile16, Val17 and Tyr18 forming the  $\beta$ -strands in each subunit have favourable  $\Delta \Delta G_{eff}$  contributions. The favourable interactions between the backbones ( $\Delta \Delta G_{cav}^{bb} < -0.85$  kcal/mol) origin from their involvement in the formation of the amide hydrogen bonds (H-bonds) with the residues located in the  $\beta$ -hairpin of  $A\beta$  or in the formation of the long-range electrostatic interactions with other charged groups (Table 2). On the other hand, some groups, such as the side chains of Ile16 and Tyr18, contribute to the effective energies through the van der Waals interactions with the hydrophobic side chains of Val18, Phe20, Ile31 and Met35 of the  $A\beta$  peptide. These residues form a hydrophobic cluster at the exterior face of  $A\beta$  (Table 2 and Fig. 2a). The side chain of  $Z_{A\beta 3}$  Tyr18 is amphiphatic, of which the -O-H group is a hydrogen bond donor and the aromatic ring likely participates in the van der Waals interactions with  $A\beta$ , leading to that its contribution to  $\Delta \Delta G_{eff}$  becomes as high as -4.96 kcal/mol (Fig. 2a). The hydrophobic residues Leu17, Leu19, Leu27 and Leu45 from both subunits also have significant contributions to the binding of  $(Z_{A\beta 3})_2$  to  $A\beta$  (Table 2). This can be explained by the fact that these residues are packed against each other and form a large hydrophobic core with the affinity residues Phe30, Ile31 and Leu34. In this way, the hydrophobic residues at the interior face of the  $\beta$ -hairpin structure become stabilized (Fig. 2b and Table S1). Some residues, such as  $Z_{A\beta 3}$  Tyr18, have large  $\Delta \Delta E_{elec}$  values, but the gain in the  $\Delta \Delta E_{elec}$  values is compensated by the unfavourable electrostatic solvation free energies ( $\Delta \Delta G_{elec,solv}$ ) originating from the screening effect of the neighboring solvent molecules.

With the nonpolar environment provided by the hydrophobic residues in the  $\alpha$ -helices, the hydrophobic groups in the central and C-terminal parts of A $\beta$  are trapped to form a  $\beta$ -hairpin structure and sealed by the N-termini of  $(Z_{A\beta 3})_2$  that form a gate-like cluster. Albeit different from the in-register and parallel tertiary structure adopted in the fibril<sup>42</sup>, the hydrophobic residues in the  $\beta$ -hairpin of A $\beta$  are involved in the formation of the  $\beta$ -strand of each A $\beta$  unit in the fibril. The  $\beta$ -strand-turn- $\beta$ -strand motifs of A $\beta$  have also been found to be stable in the trimers and higher-order oligomers mainly due to the hydrophobic contacts<sup>43</sup>. The presence of the four-strand antiparallel  $\beta$ -sheet likely suggests the formation of metastable and on-pathway A $\beta$  oligomers in the hydrophobic environment, such as in a membrane.

### Computational alanine/glycine scanning on the $(Z_{A\beta 3})_2$ residues

Results of computational alanine scanning for  $(Z_{A\beta 3})_2$  residues are given in **Fig. 3**. A positive  $\Delta\Delta G_{bind}$  value means that the residue is energetically more favourable compared with the corresponding alanine residue. Mutated residues are classified as hot spots if the mutation to alanine results in a change in  $\Delta\Delta G_{bind}$  larger than 2.0 kcal/mol.

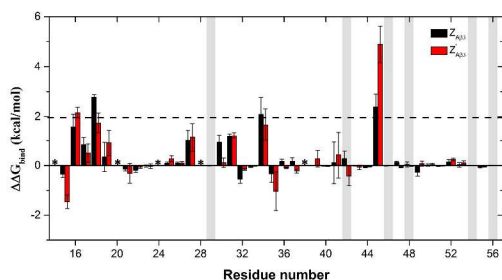


**Figure 3.**  $\Delta\Delta G_{bind}$  for each mutated residue of  $(Z_{A\beta 3})_2$  obtained from computational alanine/glycine scanning. The error bar for each residue was the standard deviation over four independent alanine/glycine scanning calculations. Gly14, Pro20, Pro24, Cys28 and Pro38 were not included in alanine/glycine scanning and are marked with the asterisks in their positions. Cys28 from both subunits were not mutated, as a covalent disulfide bond is formed between the thiol groups.  $\Delta\Delta G_{bind}$  values for the 6 glycine-replaced alanine residues in each subunit are highlighted by the light grey background.

The  $\Delta\Delta G_{bind}$  values were calculated for all the residues in  $(Z_{A\beta 3})_2$ , except for glycine, proline and cysteine. 5 residues with  $\Delta\Delta G_{bind} > 2$  kcal/mol were considered as hot spots and were found to be located at the  $(Z_{A\beta 3})_2$ :A $\beta$  binding interface. Of these 5 hot-spot residues, 4 were found to have hydrophobic groups. One of the residues, Leu45 from the  $Z'_{A\beta 3}$  subunit, has an extraordinary contribution to the binding of  $(Z_{A\beta 3})_2$  to A $\beta$ , with the  $\Delta\Delta G_{bind}$  value larger than 4.0 kcal/mol. As discussed in the per-residue method, the side chains of Ile16 and Tyr18, which form the  $\beta$ -strands of the  $Z_{A\beta 3}$  and  $Z'_{A\beta 3}$  subunits, have favourable energetic contributions, though  $Z_{A\beta 3}$  Ile16 and  $Z'_{A\beta 3}$  Tyr18 have  $\Delta\Delta G_{bind}$  values smaller than 2 kcal/mol. Leu34 and Leu45 of  $Z_{A\beta 3}$  are in helices  $\alpha 2$  and  $\alpha 3$ , respectively. Mutation of these two residues to alanine attenuates the energy contribution to the binding by 2.09 and 2.39 kcal/mol. It is noteworthy that Glu15 in the  $Z_{A\beta 3}$  subunit contributes

negligibly to  $\Delta\Delta G_{bind}$ . In the  $Z'_{A\beta 3}$  subunit, E15A mutation has the  $\Delta\Delta G_{bind}$  value of -1.46 kcal/mol, implying that compared with the methyl group of the alanine residue, the negatively charged side chain of Glu15 has a less favourable energy contribution to the binding of  $(Z_{A\beta 3})_2$  to A $\beta$ . The  $\Delta\Delta G_{bind}$  values of Glu15 in the  $Z_{A\beta 3}$  and  $Z'_{A\beta 3}$  subunits are also in line with the results obtained from the per-residue method (with  $\Delta\Delta G_{eff}^{SC}$  values of -0.07 and 0.06 kcal/mol, respectively), but differ from the NMR result, which indicates that the side chain of Glu15 forms a salt bridge with the positively charged  $\epsilon$ -amino group of Lys49 on each subunit<sup>20</sup>. For other residues, such as Phe30 from  $\alpha 2$  of the  $Z_{A\beta 3}$  subunit, Leu34 from  $\alpha 3$  of the  $Z'_{A\beta 3}$  subunit, and Leu27 and Ile31 from both subunits have the  $\Delta\Delta G_{bind}$  values larger than 1.0 kcal/mol, suggesting notable contributions of these hydrophobic side chains to the binding (**Fig. 2b**). For the 12 glycine-replaced alanine residues, the calculated  $\Delta\Delta G_{bind}$  values range from -0.42 to 0.28 kcal/mol, reflecting the weak effect of these methyl groups on  $(Z_{A\beta 3})_2$ :A $\beta$  formation. These values seem to be reasonable, because all the alanine residues are far away from the contact interface and are not engaged in the hydrophobic interactions with the hot spot residues. Through the above analyses, we can conclude that it is the hydrophobic residues residing in the binding interface between  $(Z_{A\beta 3})_2$  and A $\beta$ , rather than the hydrophilic residues, that contribute predominately to the  $(Z_{A\beta 3})_2$ :A $\beta$  formation. This phenomenon is also found in other protein-protein interaction studies<sup>44, 45</sup>.

Here, we compare the  $\Delta\Delta G_{bind}$  values obtained from the computational alanine scanning with the  $\Delta\Delta G_{eff}^{SC}$  values from the per-residue calculations. As can be seen in **Fig. S2**, the square of the correlation coefficient is around 0.66, meaning that the two theoretical approaches have a good correlation in estimating the energy contribution from individual residues.  $Z_{A\beta 3}$  Tyr18 and  $Z'_{A\beta 3}$  Leu45 are far away from the fitted line and look like outliers. However, both methods confirm the significant contributions of the side chain groups of the two residues, as seen by the unsigned values being larger than 2.0 kcal/mol. Therefore, the two approaches are in line with each other in characterizing the side chain contributions to the  $(Z_{A\beta 3})_2$ :A $\beta$  formation.

### Important noncovalent interactions: hydrogen-bonding and $\pi$ - $\pi$ stacking

In view of the stable 4-strand  $\beta$ -sheet formed in the complex, we study the hydrogen-bonding (H-bonding) interactions between the  $(Z_{A\beta 3})_2$  and A $\beta$  residues. An H-bond is believed to be formed if the distance between the H-bond donor (heavy atom) and receptor is less than 3.2 Å and a donor-hydrogen-acceptor angle larger than 120°. We only consider the H-bonds with the occupation rates larger than 50% during the whole simulation time.

Important H-bonds formed between the  $(Z_{A\beta 3})_2$  and A $\beta$  residues are listed in **Table 3**. Intra-molecular H-bonds formed between the backbone atoms of the A $\beta$  residues are also listed in the table, as they are engaged in forming the stable  $\beta$ -hairpin structure in the protein complex. As can be seen from the table, the  $Z_{A\beta 3}$  residues hydrogen-bonded to the carbonyl oxygen or amide nitrogen atoms of the A $\beta$  residues are the same as the residues in  $Z'_{A\beta 3}$  that are hydrogen-bonded to the corresponding A $\beta$  residues. With the exception of Glu15 on  $Z'_{A\beta 3}$ , these residues have H-binding occupation rates larger than 80% and

are found to be partially or fully surrounded by the hydrophobic groups, making the corresponding H-bonds much stronger than the one formed by Glu15 of  $Z'_{A\beta 3}$  and  $A\beta$  Asp23, which is exposed completely to the solvent and leads to a low H-bond occupation rate (10.46%) (Fig. S3). For similar reasons, the main chain atoms of the  $A\beta$  residues 18-22 and 31-35 form favourable intra-molecular H-bonds to stabilize the central strands (Fig. S4). Two strong H-bonds formed in the loop residues 24-29 were also found, with which the loop region can be immobilized to some extent, as revealed by the small RMSF values (Fig. 1b). Through the alternative intra-molecular and intermolecular H-bonds formed for each of the residues in the central  $\beta$ -strands, a four-strand antiparallel  $\beta$ -sheet is constituted through binding to the edge of the  $\beta$ -strand of each affibody subunit.

**Table 3.** Important intra-molecular and intermolecular H-bonds formed in the  $\beta$ -sheet structure.

Receptor-Donor <sup>a</sup>	Occupation rate (%)	<Distance> (Å)	Receptor-Donor <sup>a</sup>	Occupation rate (%)	<Distance> (Å)
Glu22-Tyr18 <sup>(E)</sup>	98.51 <sup>b</sup>	2.68	Met35-Val18	98.00	2.89
Val17 <sup>(E)</sup> -Leu34	98.19	2.91	Glu22-Ile31	97.71	2.91
Ile32-Leu19 <sup>(E)</sup>	97.97	2.87	Phe20-Gly33	96.57	2.90
Leu34-Val17 <sup>(E)</sup>	95.98	2.93	Val18-Met35	96.02	2.93
Glu15 <sup>(E)</sup> -Val36	71.18	2.99	Gly29-Val24	93.43	2.90
Ala21-Val17 <sup>(E)</sup>	97.04	2.91	Ile31-Glu22	92.65	2.96
Val17 <sup>(E)</sup> -Ala21	94.67	2.94	Gly33-Phe20	82.55	2.98
Phe19-Leu19 <sup>(E)</sup>	84.05	2.97	Gly25-Gly29	78.50	2.91

Only strong (with the occupation rate of 75-100%) and medium (with the occupation rate of 50-75%) H-bonds are listed above. Brackets denote that the distances were averaged over 200-ns of the first MD trajectory. Intermolecular and intra-molecular H-bonds are shown on the left and right sides of the table, respectively.

<sup>a</sup>Residues ahead and behind of the dash are H-bonding receptor and donor residues, respectively. <sup>b</sup>The -OH group on the side chain of Tyr18 can be hydrogen-bonded to each of the carboxylic oxygen atoms of  $A\beta$  Glu22 and the occupation rate is therefore the sum of the contributions from the two carboxylic oxygen atoms.

(E),(F) denote the chain names of the  $Z_{A\beta 3}$  and  $Z'_{A\beta 3}$  subunits, respectively.

It is interesting to find that for both the intra-molecular and intermolecular amide H-bonding interactions, the higher the occupation rate of an H-bond, the closer the distance between the binding partners. Moreover, the average distances for the intra-molecular H-bonds are very close to those for the intermolecular backbone H-bonds, all ranging from 2.87 to 2.99 Å. These values agree well with the N-O distances from 2.872 to 2.895 Å found in protein crystal structures<sup>46</sup>. For the H-bond formed between the -OH group on the side chain of  $Z_{A\beta 3}$  Tyr18 and the carboxylic oxygen atoms of  $A\beta$  Glu22, the occupation rate is as high as 98.51% and the average H-bond distance is shorter than the main chain H-bonds, suggesting that the H-bonding effect is very strong and the  $\beta$ -sheet structure is highly stable.

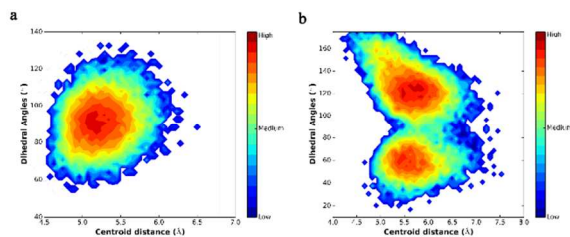


**Figure 4.** Probability distributions for the  $\pi$ - $\pi$  stacking between the side chains of the relevant residues. Distributions with respect to the centroid distance and dihedral angles formed between the  $Z_{A\beta 3}$  Tyr18 and  $A\beta$  Phe20 aromatic rings (a) and between the  $Z'_{A\beta 3}$  Tyr18 and  $A\beta$  Phe20 aromatic side chains (b), obtained from the 200 ns of the first MD trajectory.

The significant energy contribution of the  $Z_{A\beta 3}$  Tyr18 side chain group to the binding originates from two parts, namely the H-bond with the carboxylic oxygen atoms of Glu22 as analysed above, and the  $\pi$ - $\pi$  interaction with the aromatic ring of  $A\beta$  Phe20.  $\pi$ - $\pi$  interactions are supposed to occur if the closest distance between any two heavy atoms of two different rings is  $<4.5$  Å and the distance between the ring centroids is  $<7.5$  Å (calculated as the center of mass (COM) of the six carbon atoms of the benzene ring for Phe and Tyr and as the COM of the five atoms of the pyrrole ring for Trp)<sup>47</sup>. Fig. 4 shows the probability distribution with respect to the centroid distance and dihedral angles calculated based on the snapshots from the 200-ns trajectory of the first MD simulation. For the  $Z_{A\beta 3}$  Tyr18 and  $A\beta$  Phe20 pair, the majority of the centroid distance distributions were found to be less than 6.0 Å, indicating the existence of  $\pi$ - $\pi$  interactions between the aromatic rings (Fig. 4a). In addition, the high probability is distributed in the region where the centroid distances vary from 5.0 to 5.5 Å and the dihedral angles fluctuate around 90°. This implies that the T-shaped or edge-to-face configuration between the phenyl rings is formed along the whole simulation trajectory<sup>47</sup>. In contrast, the distance between the COMs of  $Z'_{A\beta 3}$  Tyr18 and  $A\beta$  Phe20 and their relative ring orientations have decentralized distributions, indicating that neither the T-shaped nor the normal parallel-displaced (with the dihedral angle equal to zero or 180°)  $\pi$ - $\pi$  interactions are formed, and the  $\pi$ - $\pi$  interactions between them are thus less strong (Fig. 4b). To determine whether a trimer is formed among the three phenyl rings,  $R_{clo}$  for each aromatic pair was recorded along the simulation trajectory. The  $R_{clo}$  values  $Z_{A\beta 3}$  Tyr18 and  $A\beta$  Phe20 are stabilized at  $\sim 3.7$  Å, and the  $R_{clo}$  values for  $Z'_{A\beta 3}$  Tyr18 and  $A\beta$  Phe20 are less stable, fluctuating at 4.5 Å, whereas the minimum distances between the two Tyr18 aromatic rings are found outside the threshold of  $\pi$ - $\pi$  interactions. Thus, we suggest that there exists only pairwise  $\pi$ - $\pi$  stacking between  $A\beta$  Phe20 and each of the Tyr18 residues (Fig. S5). The existence of  $\pi$ - $\pi$  stacking and the strong H-bond formed between the -OH group of  $Z_{A\beta 3}$  Tyr18 and the carboxylic oxygen atoms of  $A\beta$  Glu22 thus explains why the  $\Delta\Delta G_{bind}$  value of  $Z_{A\beta 3}$  Tyr18 is larger than that of  $Z'_{A\beta 3}$  Tyr18 where only weak  $\pi$ - $\pi$  stacking was found. Through the above analyses, we can conclude that it is the hydrophobic residues residing in the binding interface between  $(Z_{A\beta 3})_2$  and  $A\beta$ , rather than the hydrophilic residues, that contribute predominately to the  $(Z_{A\beta 3})_2:A\beta$  formation. This phenomenon is also found in other protein-protein interaction studies<sup>44, 45</sup>.

## Conclusions

Motivated by a recent research using the affibody  $(Z_{A\beta 3})_2$  to inhibit  $A\beta$  peptides associated with Alzheimer's disease, we have in this work carried out unbiased molecular dynamics simulations to study the binding of the affibody to  $A\beta$ . Based on the snapshots from the simulations, the effective binding free energy between  $(Z_{A\beta 3})_2$  and

$\text{A}\beta$  was computed by the MM-PBSA approach. Per-residue decomposition indicates that the  $(Z_{\text{A}\beta 3})_2$  residues contributing significantly to the binding of  $(Z_{\text{A}\beta 3})_2$  to  $\text{A}\beta$  are those engaged in the van der Waals interactions through the hydrophobic side chain groups. To find out the hot spots on the  $(Z_{\text{A}\beta 3})_2$  protein, computational alanine scanning was also carried out. 5 residues were identified with  $\Delta\Delta G_{\text{bind}}$  exceeding 2.0 kcal/mol. Of these hot spots, 4 were found to have hydrophobic groups, revealing the importance of the hydrophobic interactions in the formation of the  $(Z_{\text{A}\beta 3})_2$ : $\text{A}\beta$  complex. Y18A in  $Z_{\text{A}\beta 3}$  is of interest due to its large  $\Delta\Delta G_{\text{bind}}$  value. The computed  $\Delta\Delta G_{\text{bind}}$  value for every mutated residue was compared to its side chain contribution ( $\Delta\Delta G_{\text{eff}}^{\text{SC}}$ ), the high correlation coefficient indicates a good correlation between the two theoretical methods in estimating the side chain contributions. We would like to point out that all the mutational studies are predictions and can be validated by future experiment. Finally, the H-bonds formed in the  $\beta$ -sheet structure and the  $\pi$ - $\pi$  stacking between the aromatic rings of  $Z_{\text{A}\beta 3}$  Tyr18 and  $\text{A}\beta$  Phe20 were also observed. The fact that most of the amide groups are buried partially or fully in the hydrophobic core reflects that there exist strong H-bonding effects in the 4-strand  $\beta$ -sheet. The energetically most favorable T-shaped conformation and the stable H-bond donated by the -OH group of the  $Z_{\text{A}\beta 3}$  Tyr18 side chain to the  $\text{A}\beta$  Glu22 carboxyl group likely explain why  $Z_{\text{A}\beta 3}$  Tyr18 has the large  $\Delta\Delta G_{\text{bind}}$  value.

In summary, the present study underlines the use of MD simulations in combination with MM-PBSA free energy calculations to provide a detailed description of the energetic contribution of the  $(Z_{\text{A}\beta 3})_2$  residues to the binding of  $(Z_{\text{A}\beta 3})_2$  to  $\text{A}\beta$  at the atomistic level. Through per-residue decomposition and computational alanine scanning, a list of important residues were identified and the origin of the binding determinants for the  $(Z_{\text{A}\beta 3})_2$ : $\text{A}\beta$  complex could be pinpointed. Our results can serve as a theoretical basis in  $(Z_{\text{A}\beta 3})_2$  protein engineering, and make it possible to increase the binding affinity of  $(Z_{\text{A}\beta 3})_2$  to the  $\text{A}\beta$  peptide through guided mutation of amino acid residues.

## Acknowledgements

The authors acknowledge support from the Swedish Foundation for Strategic Research (SSF) through the project "New imaging biomarkers in early diagnosis and treatment of Alzheimer's disease". Xu Wang acknowledges the China Scholarship Council for financial support.

Division of Theoretical Chemistry and Biology, School of Biotechnology, KTH Royal Institute of Technology, S-106 91 Stockholm, Sweden.

Electronic Supplementary Information (ESI) available: [5 figures and a table show the additional information details].

## References

- H. W. Querfurth and F. M. LaFerla, *N. Engl. J. Med.*, 2010, 362, 329-344.
- G. G. Glenner and C. W. Wong, *Biochem. Biophys. Res. Commun.*, 1984, 120, 885-890.
- C. L. Masters, G. Multhaup, G. Simms, J. Pottgiesser, R. Martins and K. Beyreuther, *EMBO J.*, 1985, 4, 2757.
- D. J. Selkoe, *Nature*, 1999, 399, A23-A31.
- K. N. Dahlgren, A. M. Manelli, W. B. Stine, L. K. Baker, G. A. Krafft and M. J. LaDu, *J. Biol. Chem.*, 2002, 277, 32046-32053.
- C. Haass and D. J. Selkoe, *Nat. Rev. Mol. Cell Biol.*, 2007, 8, 101-112.
- D. M. Walsh, I. Klyubin, J. V. Fadeeva, W. K. Cullen, R. Anwyl, M. S. Wolfe, M. J. Rowan and D. J. Selkoe, *Nature*, 2002, 416, 535-539.
- G. M. Shankar, S. Li, T. H. Mehta, A. Garcia-Munoz, N. E. Shepardson, I. Smith, F. M. Brett, M. A. Farrell, M. J. Rowan and C. A. Lemere, *Nat. Med.*, 2008, 14, 837-842.
- K. Ono, M. M. Condon and D. B. Teplow, *Proc. Natl. Acad. Sci. USA*, 2009, 106, 14745-14750.
- T. Hård and C. Lendel, *J. Mol. Biol.*, 2012, 421, 441-465.
- D. Schenk, R. Barbour, W. Dunn, G. Gordon, H. Grajeda, T. Guido, K. Hu, J. P. Huang, K. Johnson-Wood, K. Khan, D. Kholodenko, M. Lee, Z. M. Liao, I. Lieberburg, R. Motter, L. Mutter, F. Soriano, G. Shopp, N. Vasquez, C. Vandever, S. Walker, M. Wogulis, T. Yednock, D. Games and P. Seubert, *Nature*, 1999, 400, 173-177.
- E. Check, *Nature*, 2002, 415, 462-462.
- C. Hock, U. Konietzko, J. R. Streffer, J. Tracy, A. Signorell, B. Muller-Tillmanns, U. Lemke, K. Henke, E. Moritz, E. Garcia, M. A. Wollmer, D. Umbricht, D. J. F. de Quervain, M. Hofmann, A. Maddalena, A. Papassotiropoulos and R. M. Nitsch, *Neuron*, 2003, 38, 547-554.
- K. Blennow, H. Zetterberg, J. O. Rinne, S. Salloway, J. Wei, R. Black, M. Grundman and E. Liu, *Arch. Neurol.*, 2012, 69, 1002-1010.
- J. O. Rinne, D. J. Brooks, M. N. Rossor, N. C. Fox, R. Bullock, W. E. Klunk, C. A. Mathis, K. Blennow, J. Barakos and A. A. Okello, *Lancet Neurol*, 2010, 9, 363-372.
- S. Salloway, R. Sperling, N. C. Fox, K. Blennow, W. Klunk, M. Raskind, M. Sabbagh, L. S. Honig, A. P. Porsteinsson and S. Ferris, *N. Engl. J. Med.*, 2014, 370, 322-333.
- C. Gronwall, A. Jonsson, S. Lindstrom, E. Gunneriusson, S. Stahl and N. Herne, *J. Biotechnol.*, 2007, 128, 162-183.
- W. Hoyer and T. Hard, *J. Mol. Biol.*, 2008, 378, 398-411.
- L. M. Luheshi, W. Hoyer, T. P. de Barros, I. van Dijk Hard, A. C. Brorsson, B. Macao, C. Persson, D. C. Crowther, D. A. Lomas, S. Stahl, C. M. Dobson and T. Hard, *PLoS Biol.*, 2010, 8, e1000334.
- W. Hoyer, C. Gronwall, A. Jonsson, S. Stahl and T. Hard, *Proc Natl Acad Sci USA*, 2008, 105, 5099-5104.
- J. Lindgren, A. Wahlstrom, J. Danielsson, N. Markova, C. Ekblad, A. Graslund, L. Abrahamson, A. E. Karlstrom and S. K. Warmlander, *Protein Sci.*, 2010, 19, 2319-2329.
- H. Lindberg, A. Johansson, T. Hard, S. Stahl and J. Lofblom, *Biotechnol. J.*, 2013, 8, 139-145.
- J. Srinivasan, T. E. Cheatham, P. Cieplak, P. A. Kollman and D. A. Case, *J. Am. Chem. Soc.*, 1998, 120, 9401-9409.
- H. Gohlke and D. A. Case, *Journal of Computational Chemistry*, 2004, 25, 238-250.
- H. Wang and C. A. Lughton, *Phys. Chem. Chem. Phys.*, 2009, 11, 10722-10728.
- H. Y. Sun, Y. Y. Li, S. Tian, L. Xu and T. J. Hou, *Phys. Chem. Chem. Phys.*, 2014, 16, 16719-16729.
- M. H. M. Olsson, C. R. Sondergaard, M. Rostkowski and J. H. Jensen, *J. Chem. Theory Comput.*, 2011, 7, 525-537.
- B. Hess, C. Kutzner, D. van der Spoel and E. Lindahl, *J. Chem. Theory Comput.*, 2008, 4, 435-447.
- K. Lindorff-Larsen, S. Piana, K. Palmo, P. Maragakis, J. L. Klepeis, R. O. Dror and D. E. Shaw, *Proteins: Structure, Function, and Bioinformatics*, 2010, 78, 1950-1958.
- W. L. Jorgensen, J. Chandrasekhar, J. D. Madura, R. W. Impey and M. L. Klein, *J. Chem. Phys.*, 1983, 79, 926-935.
- G. Bussi, D. Donadio and M. Parrinello, *J. Chem. Phys.*, 2007, 126, 014101.
- B. Hess, H. Bekker, H. J. C. Berendsen and J. G. E. M. Fraaije, *J. Comput. Chem.*, 1997, 18, 1463-1472.
- M. Parrinello and A. Rahman, *J. Appl. Phys.*, 1981, 52, 7182-7190.
- D. A. Case, T. E. Cheatham, T. Darden, H. Gohlke, R. Luo, K. M. Merz, A. Onufriev, C. Simmerling, B. Wang and R. J. Woods, *J. Comput. Chem.*, 2005, 26, 1668-1688.
- T. J. Hou, J. M. Wang, Y. Y. Li and W. Wang, *J. Chem. Inf. Model.*, 2011, 51, 69-82.

- 36 J. M. Wang, P. Morin, W. Wang and P. A. Kollman, *J. Am. Chem. Soc.*, 2001, 123, 5221-5230.
- 37 C. Tan, Y. H. Tan and R. Luo, *J. Phys. Chem. B*, 2007, 111, 12263-12274.
- 38 C. H. Tan, L. J. Yang and R. Luo, *J. Phys. Chem. B*, 2006, 110, 18680-18687.
- 39 B. R. Miller, T. D. McGee, J. M. Swails, N. Homeyer, H. Gohlke and A. E. Roitberg, *J. Chem. Theory Comput.*, 2012, 8, 3314-3321.
- 40 S. Huo, I. Massova and P. A. Kollman, *J. Comput. Chem.*, 2002, 23, 15-27.
- 41 N. Homeyer and H. Gohlke, *Mol. Inform.*, 2012, 31, 114-122.
- 42 A. T. Petkova, W. M. Yau and R. Tycko, *Biochemistry*, 2006, 45, 498-512.
- 43 R. K. Spencer, H. Li and J. S. Nowick, *J. Am. Chem. Soc.*, 2014, 136, 5595-5598.
- 44 S. Jakobi, T. X. P. Nguyen, F. Debaene, A. Metz, S. Sanglier-Cianferani, K. Reuter and G. Klebe, *Proteins: Structure Function and Bioinformatics*, 2014, 82, 2713-2732.
- 45 N. J. Deng and P. Cieplak, *Phys. Chem. Chem. Phys.*, 2009, 11, 4968-4981.
- 46 G. A. Jeffrey and W. Saenger, *Hydrogen Bonding in Biological Structures*, Springer, Berlin, 1991.
- 47 G. B. McGaughey, M. Gagné and A. K. Rappé, *J. Biol. Chem.*, 1998, 273, 15458-15463.